UC San Diego

UC San Diego Previously Published Works

Title

A Probabilistic Model for Quantifying Uncertainty of Acoustic Nonlinearities of Lamb Waves and Its Application to the Characterization of Damage in Composite Laminates

Permalink

https://escholarship.org/uc/item/29f9j4n1

Authors

HONG, MING
MAO, ZHU
TODD, MICHAEL
et al.

Publication Date

2015

DOI

10.12783/shm2015/281

Peer reviewed

COVER SHEET

Title: A Probabilistic Model for Quantifying Uncertainty of Acoustic Nonlinearities of Lamb Waves and Its Application to the Characterization of Damage in Composite Laminates

Authors (names are for example only): Ming Hong
Zhu Mao
Michael D. Todd
Zhongqing Su
Xinlin Qing

PAPER DEADLINE: **May 15, 2015**

PAPER LENGTH: **8 PAGES MAXIMUM **

Please submit your paper in PDF format. We encourage you to read attached Guidelines prior to preparing your paper—this will ensure your paper is consistent with the format of the articles in the CD-ROM.

NOTE: Sample guidelines are shown with the correct margins. Follow the style from these guidelines for your page format.

Hardcopy submission: Pages can be output on a high-grade white bond paper with adherence to the specified margins (8.5 x 11 inch paper. Adjust outside margins if using A4 paper). Please number your pages in light pencil or non-photo blue pencil at the bottom.

Electronic file submission: When making your final PDF for submission make sure the box at "Printed Optimized PDF" is checked. Also—in Distiller—make certain all fonts are embedded in the document before making the final PDF.

ABSTRACT

Nonlinear Lamb wave features are known to be sensitive to microscopic damage, such as fatigue, creep, and material thermal degradation. While previous studies have shown their effectiveness in detecting undersized damage in metallic materials, this study aims to extend the use of the relative acoustic nonlinearity parameter (RANP), a prominent nonlinear feature, to damage characterization in composite materials. First, principles of nonlinear ultrasonics are revisited briefly. Considering operational and measurement uncertainties, it is desirable to quantify the uncertainty of RANP (i.e., its statistics) to facilitate damage characterization. In doing so, an analytical model is established to numerically evaluate the distribution of RANP. Using piezoelectric wafers, continuous sine waves are generated in carbon fiber plate samples. Steady-state responses are acquired and processed to produce the histograms of RANP estimates, in both healthy and damaged conditions, to which the analytical probability model is fit. These distributions are used to enhance the robustness of the parameter, and impact damage in the composite sample is evaluated. The results have shown good agreement between the model and experimental data, and have provided a quantified level of confidence in using RANP for damage state classification in composites.

INTRODUCTION

Composite materials have been increasingly utilized to build engineering structures and systems, especially in the aerospace and transportation industries. Featuring high strength-to-weight ratios, these materials may nevertheless suffer various forms of damage that are invisible or difficult to identify, primarily due to their susceptibility to foreign object impacts [1]. For example, low-velocity impacts, such as tool dropping

Ming Hong, Dept. of Mechanical Engineering, The Hong Kong Polytechnic University, Hong Kong, China, and Dept. of Structural Engineering, University of California San Diego, USA
Zhu Mao, Dept. of Structural Engineering, University of California San Diego, USA
Michael D. Todd, Dept. of Structural Engineering, University of California San Diego, USA
Zhongqing Su, Dept. of Mechanical Engineering, The Hong Kong Polytechnic University, Hong Kong, China
Xinlin Qing, Division of Aviation Health Safety Management, Beijing Aeronautical Science and Technology Research Institute, COMAC, China

during the manufacturing and servicing stages, may result in what is commonly referred to as *barely visible impact damage* (BVID). Typical types of BVID range from indentation and matrix micro-cracks to ply delamination and fiber breakage.

Over the years, many nondestructive evaluation (NDE) methods and structural health monitoring (SHM) systems based on Lamb waves have been developed for damage detection in composite laminates. However, majority of the past efforts has been targeted at analyzing linear property variations induced by structural damage. As discussed in other works [1, 2], these linear techniques may not be appropriate to apply to inhomogeneous materials and structures with small-scale damage, which is usually the case for composite materials. On the other hand, nonlinear Lamb wave features have demonstrated their higher sensitivities to micro-defects that are common in composite materials. Aymerich and Staszewski [3] and Meo et al. [4] adopted a technique called nonlinear elastic wave spectroscopy to evaluate BVID in composite structures. Pieczonka et al. [5] studied the effectiveness of second harmonic generation and compared it to local defect resonance when assessing the imaging quality of BVID. Li et al. [6] then used the *relative acoustic nonlinearity parameter* (RANP) extracted from second harmonic Lamb waves to detect thermal fatigue damage in a composite panel.

In some aforementioned studies, the effectiveness of RANP has been illustrated for damage detection in composites. However, uncertainties are always associated with any signal feature employed for SHM, which may obfuscate or even bias the result. Thus, it is always necessary to consider the uncertainties inherent in measurement, operation, ambient conditions, and/or computation [7], any of which may impair the user's ability to interpret the detection outcome. To avoid making excessive Type I or Type II errors in the damage identification process, the uncertainties involved in RANP must be quantified, so that statistical inference may be made on the structural condition.

In this backdrop, this study attempts to establish a probability model to quantify the uncertainty of RANP estimates of Lamb waves, which are collected from composite materials before and after the introduction of BVID. Experiments are performed on a carbon fiber/epoxy (CF/EP) plate using piezoelectric wafers. Continuous sine waves are generated as the input, and steady-state signals are acquired for calculating RANP. Histograms and predicted distributions of RANP before and after the introduction of BVID are compared, and a receiver operating characteristic (ROC) curve is obtained, which provides a quantified level of confidence for damage state classification.

SECOND HARMONICS OF LAMB WAVES

Lamb waves are the type of guided waves confined in thin plates. Specifically, nonlinear Lamb waves pertain to scenarios where extra frequency bands, other than at the excitation frequency, are found in the acquired signals. In particular, second harmonics refers to the wave formation at twice the excitation frequency, due to nonlinear variations of material properties (i.e., small-scale damage, typically quadratic in nature). Theoretically, the generation of second harmonics can be considered a first-order perturbation to the linear elastic response [6]. As a result, the solution to the nonlinear wave equation consists of two parts: the fundamental mode at the excitation frequency ω, plus the perturbed second harmonic mode at 2ω. The amplitudes of the two modes are related by the acoustic nonlinearity parameter, or β, defined as

$$\beta = \frac{A_2}{A_1^2} \frac{8}{k^2 x} \gamma, \tag{1}$$

where A_1 and A_2 are the amplitudes at ω and 2ω, respectively; k is the wavenumber, x is the propagation distance, and γ is a function depending on wave parameters and medium properties [8], which does not vary with the health condition of the structure. Based on this equation, the degree of second harmonic generation (hence the degree of nonlinearities in the inspected structure) may be determined. Normalizing β at a fixed k and x (while γ remains unchanged), Eq. (1) may be simplified into

$$RANP = \frac{A_2}{A_1^2}, \tag{2}$$

which defines the RANP as the parameter investigated in this paper.

Due to the multimodal and dispersive natures of Lamb waves, their second harmonic effect is usually very weak. However, there exist certain conditions under which the second harmonic generation is cumulative with propagation distance. In principle, if the fundamental mode and a second harmonic mode share the same phase velocity, and provided with non-zero power flux, internal resonance occurs and energy can be transferred from the fundamental mode to the second harmonics continuously. Thus, by selecting a specific excitation frequency that enables internal resonance, cumulative second harmonics can be generated, ensuring a higher signal-to-noise ratio for signal processing purposes.

The dispersion curves for a unidirectional CF/EP plate [0]$_8$ (thickness: 1.588 mm, tensile modulus in the fiber direction: 120.66 GPa, density: 1,410 kg/m^3) are displayed in Figure 1. According to the internal resonance conditions, mode pair (S1, S2) is identified as an eligible combination for cumulative second harmonic generation.

A PROBABILISTIC MODEL OF RANP ESTIMATION

The amplitudes A_1 and A_2 in Eq. (2) can be found in the signal's spectrum after fast Fourier transform (FFT). Following the procedure of FFT, Eq. (2) can be rewritten as

$$RANP = \frac{\sqrt{Y_{2r}^2 + Y_{2i}^2}}{Y_{1r}^2 + Y_{1i}^2}, \tag{3}$$

where Y_{1r}, Y_{1i}, Y_{2r}, and Y_{2i} are the real and imaginary parts of the signal after FFT at ω
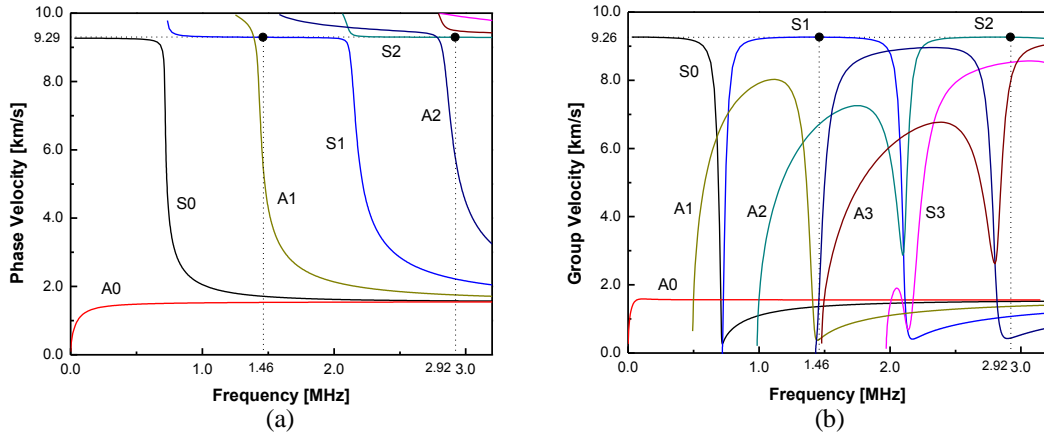

Figure 1. Dispersion curves of CF/EP laminate [0]$_8$ (thickness: 1.588 mm): (a) phase velocities; (b) group velocities. Mode pair (S1, S2) is marked for cumulative second harmonic generation.

and 2ω, respectively. For a given frequency component of the spectrum, the fundamental uncertainty in each of its real and imaginary parts is assumed to follow a statistically independent normal distribution. These two normal distributions have the same standard deviation but different means, i.e., $Y_r \sim N(\mu_r, \sigma^2)$, $Y_i \sim N(\mu_i, \sigma^2)$, and $Y_r \perp Y_i$, as the FFT maps the same original time series onto two orthogonal domains without discriminating the transformation gain.

Therefore, for the numerator in Eq. (3), $Y_{2r} \sim N(\mu_{2r}, \sigma_2^2)$ and $Y_{2i} \sim N(\mu_{2i}, \sigma_2^2)$, where σ_2 is the common standard deviation at 2ω. Hence, the random variable A_2 can be assumed to follow a Rice distribution. Similarly, for the denominator, we assume $Y_{1r} \sim N(\mu_{1r}, \sigma_1^2)$ and $Y_{1r} \sim N(\mu_{1r}, \sigma_1^2)$, where σ_1 is the common standard deviation at ω. The random variable A_1^2 / σ_1^2, which is the squared amplitude scaled by a constant, then follows a noncentral chi-square distribution. Now, assuming these two random variables do not depend on each other from the perspective of signal processing, the joint probability density function (PDF) of $X_1 = A_1^2 / \sigma_1^2$ and $X_2 = A_2$ becomes

$$
\begin{aligned}
p_{X_1,X_2}(x_1,x_2) &= p_{X_1}(x_1)\,p_{X_2}(x_2) \\
&= \frac{x_2}{2\sigma_2^2}\exp\!\left(-\frac{x_1+\lambda_n}{2}-\frac{x_2^2+v_n^2}{2\sigma_2^2}\right)I_0\!\left(\sqrt{\lambda_n x_1}\right)I_0\!\left(\frac{x_2 v_n}{\sigma_2^2}\right),
\end{aligned}
\tag{4}
$$

where $p_{X_1}(x_1)$ and $p_{X_2}(x_2)$ are the PDFs of the noncentral chi-square distribution and the Rice distribution, respectively; λ_n and v_n are the distributions' noncentrality parameters, and $I_0(.)$ is the zero-order modified Bessel function of the first kind. Thus, the distribution of the ratio $R = X_2 / X_1$ is characterized as

$$
p_R(r) = \frac{d}{dr}\left[\mathrm{Prob}\!\left(\frac{X_2}{X_1}<r\right)\right] = \frac{d}{dr}\int_0^{+\infty}\int_0^{rx_1} p_{X_1,X_2}(x_1,x_2)\,dx_2\,dx_1 .
\tag{5}
$$

Finally, substituting Eq. (4) into Eq. (5) yields

$$
p_R(r) = \int_0^{+\infty}\frac{x_1^2 r}{2\sigma_2^2}\exp\!\left(-\frac{x_1+\lambda_n}{2}-\frac{x_1^2 r^2+v_n^2}{2\sigma_2^2}\right)I_0\!\left(\sqrt{x_1\lambda_n}\right)I_0\!\left(\frac{x_1 v_n r}{\sigma_2^2}\right)dx_1 ,
\tag{6}
$$

which does not have a further known closed-form solution. Instead, it can be evaluated numerically once the values λ_n, σ_2, and v_n are retrieved from experimental data,. Figure 2 shows representative plots of the PDF and the cumulative density function (CDF) of the ratio R using arbitrary parametric values. The distribution of RANP then can be obtained by scaling the axes for this PDF by an adjusted (average) σ_1^2.
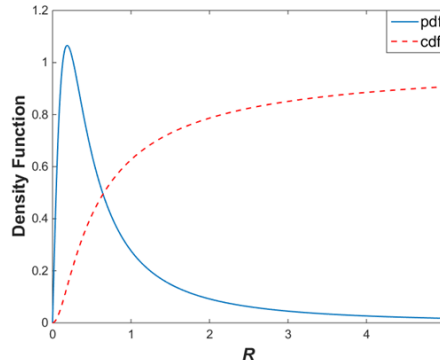

Figure 2. PDF and CDF of R, with $\lambda_n = 0.6$, $\sigma_2 = 1$, and $v_n = 0.5$.

EXPERIMENT AND UNCERTAINTY QUANTIFICATION

Healthy Condition

The proposed probability model of RANP is validated on a CF/EP sample, whose schematic diagram is shown in Figure 3(a). Material specifications and its dispersion curves have been given earlier. Two lead zirconate titanate (PZT) wafers, 10 mm in diameter each, are mounted on the plate to configure a sensing path along the fiber direction. According to Figure 1, the frequency of 1.46 MHz is selected for cumulative second harmonic generation, at which S1 is excited as the fundamental mode (among other modes). In order to have output signals as stationary as possible, a continuous sine wave is generated. This stationary input signal would lead to a steady-state response at the sensor as a result of superposition of all Lamb wave modes in the structure, including S2 due to nonlinearities. It has been assumed earlier that both the real and imaginary parts of the output signal at any frequency line follow normal distributions with the same standard deviation. Thus, the stationarity of output signals will directly determine the quality of the probabilistic modeling.

As displayed in Figure 3(b), the input signal is amplified with a power amplifier before going into the actuator. Output signals are acquired at the other PZT wafer using a PXI platform at a sampling rate of 25 MHz. 500 acquisitions, each with a length of 16,384 points, are performed at random intervals, where uncertainties concerned mainly come from measurement and computation. After FFT of each of the 500 signals, their frequency-domain statistics of interest are calculated and tabulated in Table I.

Figure 4(a) shows the normalized histogram of RANP estimates from the 500 signals acquired in the healthy condition, superimposed with the predicted distribution defined by Eq. (6) using parameter values from Table I. As can be seen, the histogram matches quite well with the prediction, which also validates the assumptions being made in deriving the PDF. It is noteworthy that the predicted PDF has an infinitely long tail extending to infinity; in contrast, the maximum RANP estimate obtained from the
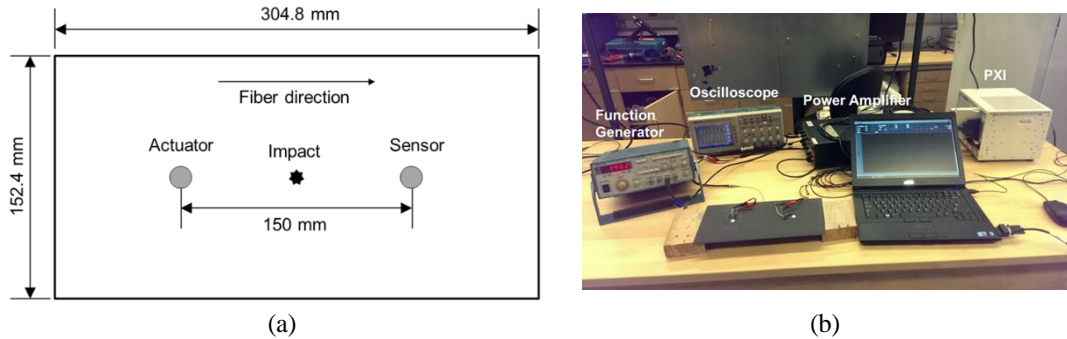

(a)   (b)

Figure 3. (a) Schematic diagram of the CF/EP plate; (b) experimental setup.

TABLE I. SIGNAL STATISTICS AFTER FFT OF 500 ACQUISITIONS

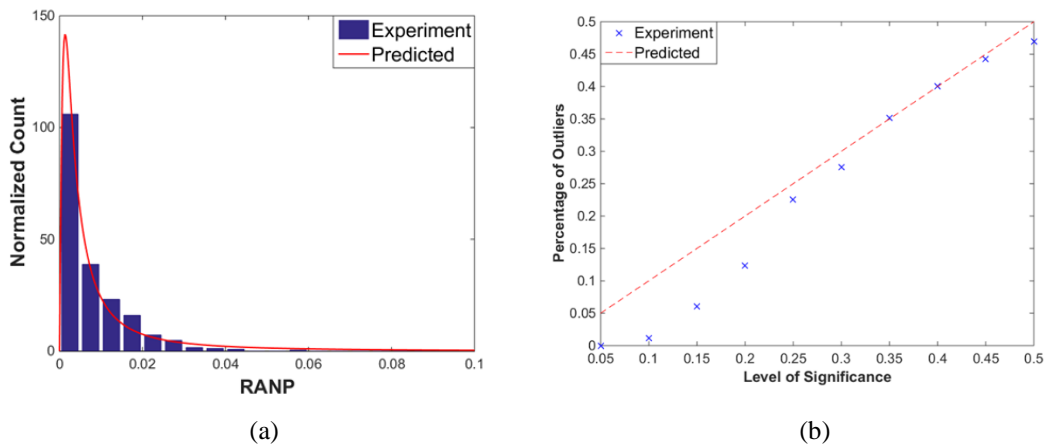| FFT Frequency	Real Part Mean μ_{1r}	Imag. Part Mean μ_{1i}	Average Std. Dev. σ_1	λ_n
1.461 MHz	0.0080	-9.953×10^{-4}	0.3898	4.297×10^{-4}
FFT Frequency	**Real Part Mean** μ_{2r}	**Imag. Part Mean** μ_{2i}	**Average Std. Dev.** σ_2	ν_n
2.922 MHz	4.598×10^{-5}	-1.052×10^{-4}	9.185×10^{-4}	1.148×10^{-4}

Figure 4. (a) RANP histogram and predicted distribution under the healthy condition; (b) Percentage of outliers against level of significance.

experiment is only 0.059. To compare more closely the two results, an outlier analysis is performed. Specifically, percentile locations of the predicted PDF in Figure 4(a) are determined (e.g., the 95th percentile in the model is located at RANP = 0.074, corresponding to a 5% significance level, or outliers of 5%). Then, actual outlier percentages at these RANP locations are calculated for the histogram. Figure 4(b) shows the plots for the prediction and experiment results. As can be seen, the outlier percentage of RANP estimates from the experiment is roughly proportional to the significance level determined by the prediction. However, deviations can also be noticed, especially at lower significance levels. This finding is most likely due to the long tail effect of the model. Nevertheless, for damage detection purposes, users of RANP estimates are mostly interested in the main body of the distribution than extreme values. The prediction captures the main body of the histogram rather well.

Damaged Condition

A drop-weight impact test is performed with a 0.3-kg impactor, in order to introduce BVID to the composite sample. It attempts to create internal damage to the material without significantly affecting the bonding conditions between the PZT wafers and the sample, which may otherwise alter signal statistics. The impact energy is estimated to be 1.46 J, which may induce matrix cracking and minor delamination in CF/EP [3]. After the test, the sample is re-instrumented, leaving all the measurement settings untouched. To confirm the occurrence of the damage, a C-scan is performed over a 100-mm by 100-mm area in the middle of the sample, and the result is shown in Figure 5(a). As can be seen, slightly to the lower right of the center point, an area of about 0.4 inch (10.2 mm) in diameter can be spotted with gold or orange pixels, compared to the rest filled with green yellow.

Once the damage is verified, another set of 500 signals is acquired and processed with exactly the same algorithm. Figure 5(b) shows both the histograms and predicted distributions before and after the occurrence of BVID. It can be seen that the histogram in the damaged case has a fatter tail, extending much further to the right than the healthy one. This represents a greater probability of having a bigger RANP estimate relative to the intact condition, which is intuitively consistent with the theory that increased nonlinearities (due to damage) will lead to an increased RANP estimate. Similarly, the two predicted distributions also capture the above distinction.
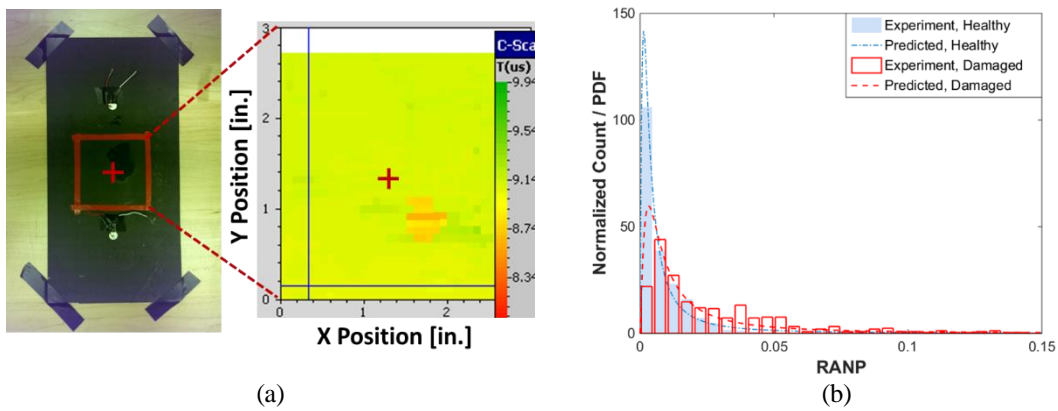
Figure 5. (a) C-scan image for the central part of the sample, highlighting the existence of the BVID; (b) histograms of RANP estimates and predicted distributions under the healthy and damaged conditions.

In order to see how the uncertainty of RANP estimates may get involved in damage identification, the concept of *receiver operating characteristics* (ROC) is adopted in this study. In Figure 6(a), two distributions, before and after damage occurrence, of some damage-related feature (e.g., RANP) are shown. The vertical line is the decision boundary: to the left, a *negative* decision (i.e., no damage) is made; to the right, a *positive* (i.e., damage existent) is called. Hence, we can define the following four detection results: True Positive (TP), False Positive (FP), True Negative (TN), and False Negative (FN), as shown by the different colors in the figure.

Now, a relationship between TP and FP can be obtained by sliding the decision boundary across the entire range of the signal feature (the horizontal axis), and the resulting plot is referred to as a ROC curve. Figure 6(b) exhibits the ROC plot obtained from the predicted RANP distributions (represented by the two PDF curves in Figure 5(b)). If the user selects a certain FP rate he or she can tolerate, a particular RANP value associated with that FP rate becomes the decision boundary. The user is thus enabled to obtain a quantified level of confidence (i.e., the TP rate) at the selected FP rate. For instance, if the tolerance for FP is 0.4 or 40%, it is expected to achieve a TP rate of roughly 70% with the next RANP estimate, using the PDFs modeled by Eq. (6). Note that the dash-dotted line across the diagonal in Figure 6(b) represents a neutral reference, meaning an equal likelihood of making a TP or FP decision all the time.
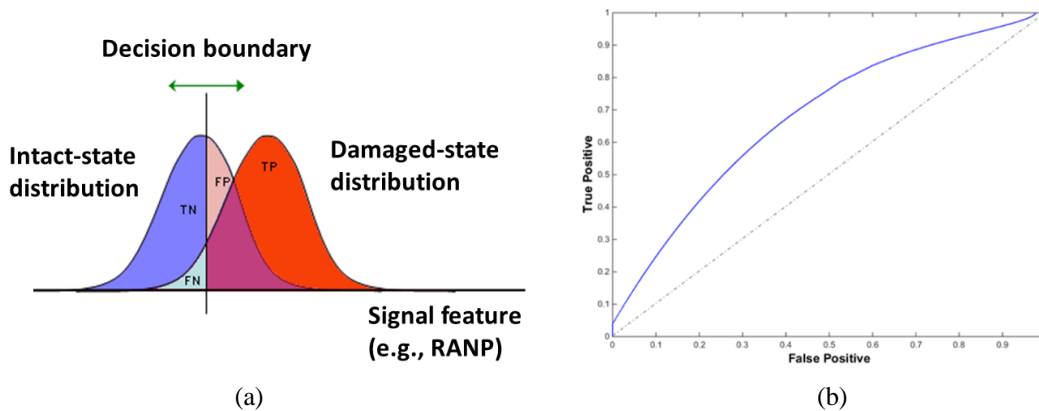

Figure 6. (a) Illustration of TP, FP, TN, and FN with respect to the two distributions; (b) ROC curve showing TP vs. FP, predicted by the modeled distributions as shown in Figure 5(b).

CONCLUSIONS

In this study, the nonlinear Lamb wave signal feature, RANP, is employed to evaluate BVID in a CF/EP laminate. While the damage is apparently identifiable by the feature, the uncertainty inherent in RANP is modeled and scrutinized.

Using a single actuator-sensor path consisting of two PZT wafers, a continuous sine wave at a selective frequency is excited. A steady-state response is achieved and processed in the frequency domain to extract necessary signal features. The modeled RANP distribution is numerically evaluated using the signal statistics, and is compared to the histogram of RANP estimates from the experiment. With BVID introduced to the sample, the new RANP distribution exhibits a fatter tail to the right, showing a greater probability of having a larger RANP estimate relative to the intact condition. This finding demonstrates the effectiveness of RANP in detecting damage-induced nonlinearities in composite materials.

Using the RANP distribution model, a ROC curve is plotted to indicate the level of confidence in making TP detections at an accepted FP rate. The ROC analysis provides a quantified reliability measure of RANP for not only BVID detection in composites, but many other scenarios of SHM where second harmonic Lamb waves are of interest.

ACKNOWLEDGMENTS

REFERENCES

1. Ciampa, F., Onder, E., Barbieri, E. and Meo, M. 2014. "Detection and modelling of nonlinear elastic response in damaged composite structures," *J. Nondestruct. Eval.*, 33: 515–521.
2. Su, Z., Zhou C., Hong, M., Cheng, L., Wang Q. and Qing, X. 2014. "Acousto-ultrasonics-based fatigue damage characterization: Linear versus nonlinear signal features," *Mech. Syst. Signal Proc.*, 45: 225–239.
3. Aymerich, F. and Staszewski, W. J. 2010. "Impact damage detection in composite laminates using nonlinear acoustics," *Compos. Part A*, 41: 1084–1092.
4. Meo M., Polimeno U. and Zumpano, G. 2008. "Detecting damage in composite material using nonlinear elastic wave spectroscopy," *Appl. Compos. Mater.*, 15: 115–126.
5. Pieczonka, L., Klepka, A., Staszewski, W. J. and Uhl, T. 2014. "Nonlinear acoustic imaging of structural damages in laminated composites," *Proc. 7th EWSHM*, 1670–1675.
6. Li, W., Cho, Y. and Achenbach, J. D. 2012. "Detection of thermal fatigue in composites by second harmonic Lamb waves," *Smart Mater. Struct.*, 21: 085019.
7. Mao, Z. and Todd, M. 2012. "A model for quantifying uncertainty in the estimation of noise-contaminated measurements of transmissibility," *Mech. Syst. Signal Proc.*,28: 470–481.
8. Xiang, Y., Deng, M., Xuan, F.-Z. and Liu, C.-J. 2011. "Experimental study of thermal degradation in ferritic Cr-Ni alloy steel plates using nonlinear Lamb waves," *NDT E. Int.*, 44: 768–774.

DEStech Publications, Inc.

CONTRIBUTING AUTHOR COPYRIGHT RELEASE FORM

As author of the chapter/contribution titled <u>Uncertainty Quantification for Relative Acoustic Nonlinearity Parameter of Lamb Waves and Its Application to Damage Characterization in Composites</u> to appear in the *Proceedings of Structural Health Monitoring 2015*, I hereby agree to the following:

1.   To grant to DEStech Publications, Inc., 439 North Duke Street, Lancaster, PA, 17602, copyright of the above named chapter/contribution (for U.S. Government employees to the extent transferable), in print, electronic, and online formats. However, the undersigned reserve the following:
a. All proprietary rights other than copyright, such as patent rights.
b. The right to use all or part of this article in future works.

DEStech Publications thereby retains full and exclusive right to publish, market, and sell this material in any and all editions, in the English language or otherwise.

1   I warrant to DEStech Publications, Inc., that I am the (an) author of the above-named chapter/contribution and that I am the (a) copyright holder of the above-named chapter/contribution granted to DEStech Publications, Inc.

2   I warrant that, where necessary and required, I have obtained written permission for the use of any and all copyrighted materials used in the above-named chapter/contribution. I understand that I am responsible for all costs of gaining written permission for use of copyrighted materials.

3   I agree to assume full liability to DEStech Publications, Inc. and its licensee, and to hold DEStech Publications, Inc. harmless for any claim or suit filed against DEStech Publications, Inc. for violation of copyrighted material used in the above-named contribution.

Please sign and date this form and retain a copy for your records. Please include original form with your chapter/paper.

Thank you for your cooperation.

Please print name: _Ming Hong_____ _____

Signed: _____Dated: __05/28/2015_____